

## Flux jump-assisted pulsed field magnetization of high- $J_c$ bulk high-temperature superconductors

M. D. Ainslie<sup>1</sup>, D. Zhou<sup>1</sup>, H. Fujishiro<sup>2</sup>, K. Takahashi<sup>2</sup>, Y-H. Shi<sup>1</sup>, J. H. Durrell<sup>1</sup>

<sup>1</sup>Bulk Superconductivity Group, Department of Engineering, University of Cambridge, Trumpington Street, Cambridge CB2 1PZ, UK

<sup>2</sup>Department of Physical Science and Materials Engineering, Faculty of Science and Engineering, Iwate University, 4-3-5 Ueda, Morioka 020-8551, Japan

E-mail: [mda36@cam.ac.uk](mailto:mda36@cam.ac.uk)

### Abstract

Investigating, predicting and optimising practical magnetization techniques for charging bulk superconductors is a crucial prerequisite to their use as high performance 'psuedo' permanent magnets. The leading technique for such magnetization is the pulsed field magnetization (PFM) technique, in which a large magnetic field is applied via an external magnetic field pulse of duration of the order of milliseconds. Recently "giant flux leaps" have been observed during charging by PFM: this effect greatly aids magnetization as flux jumps occur in the superconductor leading to magnetic flux suddenly intruding into the centre of the superconductor. This results in a large increase in the measured trapped field at the centre of the top surface of the bulk sample and full magnetization. Due to the complex nature of the magnetic flux dynamics during the PFM process simple analytical methods, such as those based on the Bean critical state model (CSM), are not applicable. Consequently, in order to successfully model this process, a multi-physical numerical model is required, including both electromagnetic and thermal considerations over short time scales. In this paper, we show that a standard numerical modelling technique, based on a 2D axisymmetric finite-element model implementing the  $H$ -formulation, can model this behaviour. In order to reproduce the observed behaviour in our model all that is required is the insertion of a bulk sample of high critical current density,  $J_c$ . We further explore the consequences of this observation by examining the applicability of the model to a range of previously reported experimental results. Our key conclusion is that the "giant flux leaps" reported by Weinstein *et al.* and others need no new physical explanation in terms of the behaviour of bulk superconductors: it is clear the "giant flux leap" or flux jump-assisted magnetisation of bulk superconductors will be a key enabling technology for practical applications.

**Keywords:** bulk superconductors, trapped field magnets, numerical modelling, pulsed field magnetization, flux jumps, finite element method (FEM) modelling

## 1. Introduction

Large, single grain (RE)BCO (where RE = rare earth or Y) bulk superconductors, acting as trapped field magnets (TFMs), are able to trap magnetic fields greater than 17 T [1,2], an order of magnitude higher than the maximum field produced by conventional permanent magnets. Such bulk superconductors can exhibit critical current densities,  $J_c$ s, of 50 kA/cm<sup>2</sup> at 1 T and 77 K, resulting in trapped fields of up to 1-1.5 T for standard Y-Ba-Cu-O (YBCO) and greater than 2 T for (RE)BCO materials [3], with 3 T the highest trapped field at 77 K so far in a 65 mm diameter Gd-Ba-Cu-O (GdBCO) sample [4]. Additionally, neutron-irradiated YBCO samples, fabricated by the so-called U/n method [5,6], containing improved broken-columnar pinning centres, have exhibited much higher  $J_c$ s (up to several hundreds of kA/cm<sup>2</sup> [5]) and trapped fields greater than 2 T at 77 K with smaller samples only 20 mm in diameter [7].

Investigating and predicting the magnetization of these materials and developing practical magnetizing techniques is crucial to using them as TFMs in a number of engineering applications, such as electrical machines [8-11], magnetic separation [12], magnetic resonance imaging, nuclear magnetic resonance [13-15], and magnetic drug delivery systems [16,17]. The current, best-known method for magnetising bulk superconductors in practical applications is the pulsed field magnetisation (PFM) technique, whereby a large magnetic field is applied via a pulse on the order of milliseconds; however, a significant issue with existing PFM techniques is that the trapped field is generally much less than that achieved in comparison to slower field cooling (FC) and zero field cooling (ZFC) magnetisation techniques, which themselves need a large magnetising coil/fixture, and hence impractical for practical applications. The world record using PFM, using a modified multi-pulse, stepwise-cooling (MMPSC) technique, is only 5.2 Tesla at 29 K [18], which is much less than the true capability of these materials as indicated above. It should be noted that at higher operating temperatures (closer to  $T_c$ , such as 77 K), fields have been trapped close to that of FC [7,19-22].

So-called “giant flux leaps” have been observed by a number of research groups investigating PFM [7,18,23-26], and more recently in unpublished experiments carried out in our own research group, where flux jumps occur in the superconductor, and magnetic flux suddenly intrudes into the centre of the superconductor, resulting in a large increase in the measured trapped field at the centre of the top surface of the bulk sample and full magnetization. Due to the complex nature of the magnetic flux dynamics during the PFM process, simple analytical methods, such as those based on the Bean critical state model (CSM), for example, are not applicable [7,27], and a multi-physical numerical model is required to include both electromagnetic and thermal considerations over a very short time scale [3]. To date, this “giant flux leap” effect observed in a number of experiments has not yet been conclusively explained and no numerical models have reproduced it.

In this paper, it is shown that this effect can be qualitatively reproduced using a standard numerical modelling technique, based on a 2D axisymmetric finite-element model implementing the **H**-formulation. This numerical model is based on previous models published by the authors, with a modified *E*-*J* power law characteristic, representing the normal state resistivity of the superconductor when  $J > J_c$ . By simply inserting a bulk sample of high  $J_c$ , as found in high quality standard samples and neutron-irradiated ones, such “giant flux leaps” or flux jumps are observed in the model, without the need for any new physics to explain the physical mechanism underlying the effect. The magnetic flux dynamics in high  $J_c$  samples, compared with normal and low  $J_c$  samples, are

examined using the numerical modelling results, which have important implications for magnetizing bulk superconductors with high trapped fields in practical technological applications.

## 2. Numerical modelling

### 2.1 Modelling framework

The numerical model used in this paper is based on the 2D axisymmetric  $\mathbf{H}$ -formulation presented in [26] for a solenoid coil magnetizing fixture without a soft iron yoke, implemented using the commercial FEM software package COMSOL Multiphysics 5.2a [28]. The general form, partial differential equation interface of COMSOL is used for the electromagnetic analysis, and the Heat Transfer module is used for the thermal analysis, which are coupled together as described in [26,29].

In the 2D axisymmetric  $\mathbf{H}$ -formulation, the governing equations are derived from Maxwell's equations – namely, Faraday's (1) and Ampere's (2) laws:

$$\nabla \times \mathbf{E} + \frac{d\mathbf{B}}{dt} = \nabla \times \mathbf{E} + \frac{d(\mu_0 \mu_r \mathbf{H})}{dt} = 0 \quad (1)$$

$$\nabla \times \mathbf{H} = \mathbf{J} \quad (2)$$

where  $\mathbf{H} = [H_r, H_z]$  represents the magnetic field components,  $\mathbf{J} = [J_\phi]$  represents the current density and  $\mathbf{E} = [E_\phi]$  represents the electric field.  $\mu_0$  is the permeability of free space. The electrical properties of the superconductor are modelled using an  $E$ - $J$  power law relation [30,31],  $E \propto J^n$ , where  $n = 20$  and is a reasonable approximation of Bean's critical state model, for which  $n \rightarrow \infty$  [3]. However, one addition to the modelling framework in this respect is the inclusion of a normal-state resistivity when the current density in the superconductor is larger than the critical current density,  $J_c$ . A modified  $E$ - $J$  power law relationship is used, as described in [32-34] and in the FC magnetization model for bulk MgB<sub>2</sub> presented in [35]. Hence, the resistivity tends towards the normal state resistivity (here  $\rho_{\text{normal}}$  is assumed to be  $3.5 \times 10^{-6} \Omega\text{m}$ ) when  $J > 2-2.5J_c$  with  $n = 20$  [34]. This gives a more reasonable value for the resistivity than the standard  $E$ - $J$  assumption in such situations, where the normalised current density,  $J/J_c$ , can be much larger than 1 during the PFM process [36]. Fig. 1 shows a comparison of the resistivity,  $\rho$ , and electric field,  $E$ , for the standard and modified  $E$ - $J$  power law relations, where  $J_c = 2 \times 10^9 \text{ A/m}^2$  is assumed, based on the  $J_c$  value of the bulk at 40 K (see Fig. 2). Fig. 1(b) also includes the different regimes of the  $E$ - $J$  curve, corresponding to thermally assisted flux flow (TAFF), flux creep and flux flow [37]. It allows us to discern whether this is a cause of the flux jumps, but also improves the convergence properties of the numerical model.

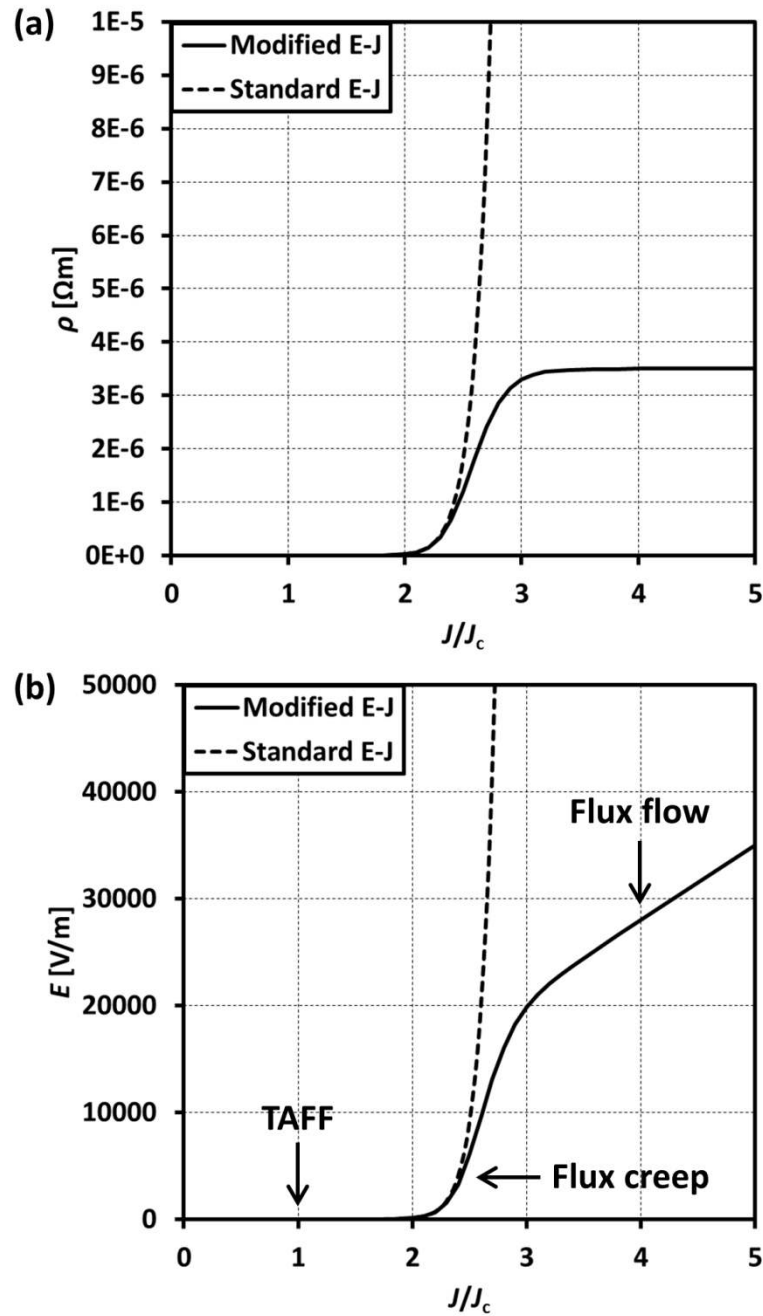


**Figure 1.** Comparison of (a) resistivity,  $\rho$ , and (b) electric field,  $E$ , for the standard  $E$ - $J$  power law relation,  $E \propto J^n$ , and the modified  $E$ - $J$  power law, where the resistivity tends towards the normal state resistivity when  $J > 2.5J_c$ . It is assumed that  $n = 20$  and  $\rho_{\text{normal}} = 3.5 \times 10^{-6}$   $\Omega\text{m}$ .

The results of the numerical model strongly depend on the  $J_c(B, T)$  characteristics of the superconductor [3], and the experimental data for  $J_c(B)$ , measured between 30-85 K from a specimen taken from a representative bulk (15 wt% Ag-containing GdBCO) is input into the model using a two-variable, direct interpolation, as described in [26,38,39]. In [26], this experimental data (up to 4 T) was fit up to 10 T using the equation presented in [40] for samples exhibiting a fishtail shape in their magnetization loop, and these  $J_c(B, T)$  characteristics are shown in Fig. 2. This method of data input is simple and direct, and can significantly improve the computational speed of the

model [38,39]. The 2D axisymmetric model assumes a homogeneous  $J_c$  distribution around the  $ab$ -plane, neglecting any effects from any inhomogeneity of  $J_c$ , e.g., [29,41-43].

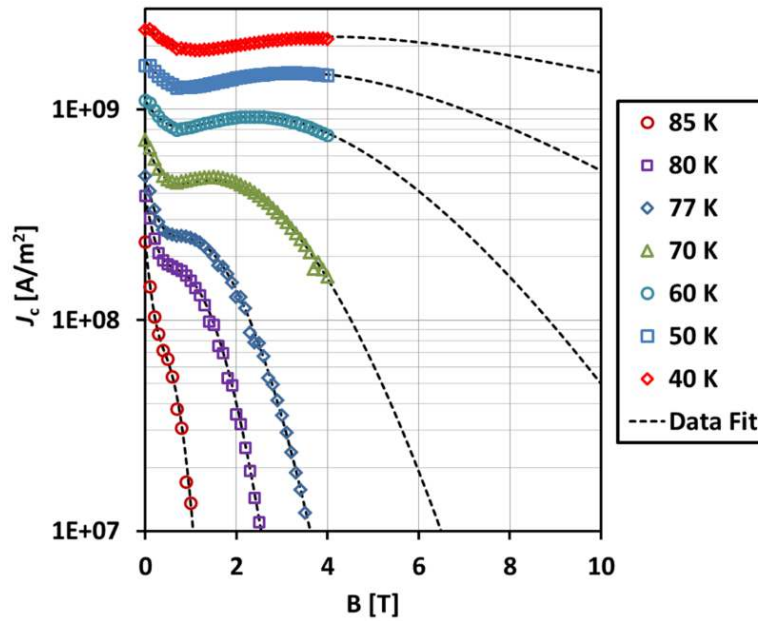


**Figure 2.** Experimental data for  $J_c(B)$ , measured from a small sample taken from a representative bulk of the same composition as the two samples (15 wt% Ag-containing Gd-Ba-Cu-O) [26]. The experimental data is fit up to 10 T using the equation presented in [40] for samples exhibiting a fishtail shape in their  $J_c(B)$  curves. © IOP Publishing. Reproduced by permission of IOP Publishing from [26]. All rights reserved.

Fig. 3 shows the 2D axisymmetric model setup for the numerical simulation. The geometry of the bulk sample is initially assumed to be 20 mm in diameter and 10 mm thickness, and as a representative magnetizing fixture, the solenoid coil experimental setup presented in [26,29] is used, with the soft iron yoke embedded in the magnetizing fixture omitted for simplicity.  $T_{op}$  is the operating temperature of the cold head, and is assumed to be 40 K in the following simulations.

Since the temperature of the superconductor can change significantly during PFM [3], the electromagnetic model is coupled with a thermal model, and the thermal behaviour is modelled using the following thermal transient equation:

$$\rho \cdot C \frac{dT}{dt} = \nabla \cdot (k \nabla T) + Q \quad (3)$$

The heat source,  $Q$ , in the thermal model is calculated from the product of the electric field and current density throughout the sample,  $Q = E_\phi \cdot J_\phi$ .

The sample is assumed to be mounted in a 316 stainless steel (SUS) sample holder with Stycast™ 2850 GT, and a thin sheet of indium, approximately 0.2 mm thick, is placed between the cold stage and the sample to ensure a good thermal contact [26]. The thermal properties (thermal conductivity and specific heat) of each of these materials, based on measured experimental data over the temperature range 0-100 K, is input into the model using a linear interpolation function [26,35]. The indium sheet has a fixed, finite thermal conductivity of  $0.5 \text{ Wm}^{-1}\text{K}^{-1}$  to represent the finite cooling

power of the refrigerator and the thermal contact between the cold stage and the bulk, as described in [44].

Pulsed currents of varying magnitude are applied to the solenoid coil via an integral constraint on the copper coil subdomain, as described in [26], such that

$$I_{pulse}(t) = N \cdot I_0 \frac{t}{\tau} \exp\left(1 - \frac{t}{\tau}\right) \quad (3)$$

where  $I_0$  is the peak magnitude of the current flowing in each turn of the solenoid coil,  $N$  is the number of turns, and  $\tau$  is the rise time of the pulse, where  $\tau = 15$  ms is assumed for each pulse. This setup has the same coil constant, relating  $B_{app}$  (the field at the centre of the magnetizing fixture with the bulk removed) to  $N \cdot I_0$  in equation (3), as presented in [26].

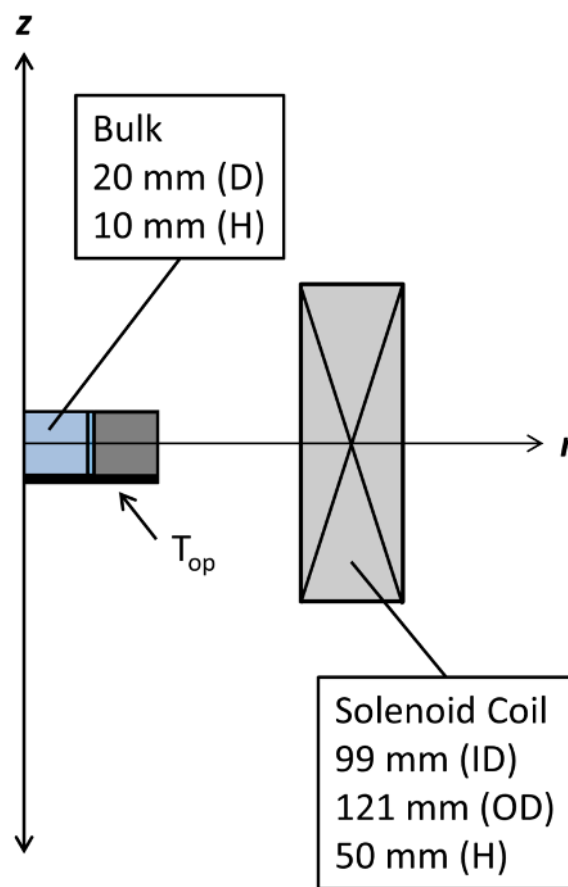


**Figure 3.** 2D axisymmetric model setup for numerical simulation of pulsed field magnetization using a solenoid coil. A thin (0.2 mm) indium sheet is placed between the bulk and cold stage to provide a good thermal contact. The bulk, which is 20 mm in diameter and of thickness 10 mm, is embedded in a 316 stainless steel (SUS) ring using Stycast™ (2850GT).  $T_{op}$  is the operating temperature of the cold head, and is assumed to be 40 K in the following simulations.

## 2.2 Simulation results

Firstly, we examine the effect of the magnitude of  $J_c$  on the simulated trapped field at the centre of the top surface of the bulk ( $z = 0.1$  mm) at  $T_{op} = 40$  K. Four samples of varying  $J_c$  are studied, with the

$J_c(B, T)$  characteristics of the representative Ag-containing GdBCO sample divided or multiplied by an integer value, which varies the magnitude of  $J_c$ , but maintains the overall pinning characteristics of the sample [22].

- Low  $J_c$        $J_c(B, T) / 3$
- Normal  $J_c$      $J_c(B, T)$
- High  $J_c$        $2J_c(B, T)$
- Ultra-High  $J_c$     $3J_c(B, T)$

Fig. 4 shows a comparison of the trapped field,  $B_t$ , at the centre of the top surface of the bulk samples ( $r = 0$  mm) at a height of  $z = 0.1$  mm at  $t = 300$  ms for applied fields,  $B_{app}$ , up to 8 T and at an operating temperature,  $T_{op}$ , of 40 K.

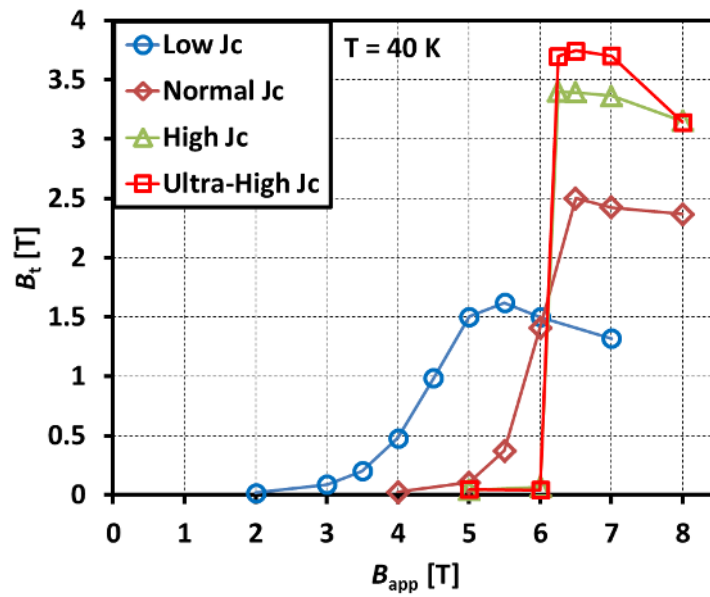


**Figure 4.** Numerical simulation results for the trapped magnetic field,  $B_t$ , at the centre of the top surface of the bulk samples ( $r = 0$  mm) at a height of  $z = 0.1$  mm at  $t = 300$  ms for applied field,  $B_{app}$ , up to 8 T and at an operating temperature,  $T_{op}$ , of 40 K.

For the high  $J_c$  and ultra-high  $J_c$  samples, there is a large increase in the trapped field at the centre of the top surface for a relatively small increase in applied field (0.25 T) above 6 T, which is qualitatively consistent with the experimental results observed in [7,18,23-26]. For the high  $J_c$  sample, for example,  $B_t$  is close to zero when  $B_{app} = 6$  T, but increases to 3.4 T when  $B_{app}$  is increased by 0.25 T to 6.25 T. For increasing  $B_{app}$  values after the sample is fully magnetized, the trapped field begins to reduce due to an increasing temperature rise generated by the rapid movement of flux lines in the sample [29].

It was observed in [24] that standard YBCO samples of a similar size to this simulated bulk, with average, in-field  $J_c$ s of 10 kA/cm<sup>2</sup> and  $B_{t,max} = 0.4$  T at 77 K, produced similar results to the simulated low and normal  $J_c$  cases, with good agreement with the CSM, as well as previously reported numerical simulation results by the authors [26,29,45]. However, high- $J_c$  samples fabricated by the U/n method, which introduces improved broken-columnar pinning centres after a sample doped with a constant mass-% of U is irradiated with thermal neutrons [24], exhibit average, in-field  $J_c$ s of

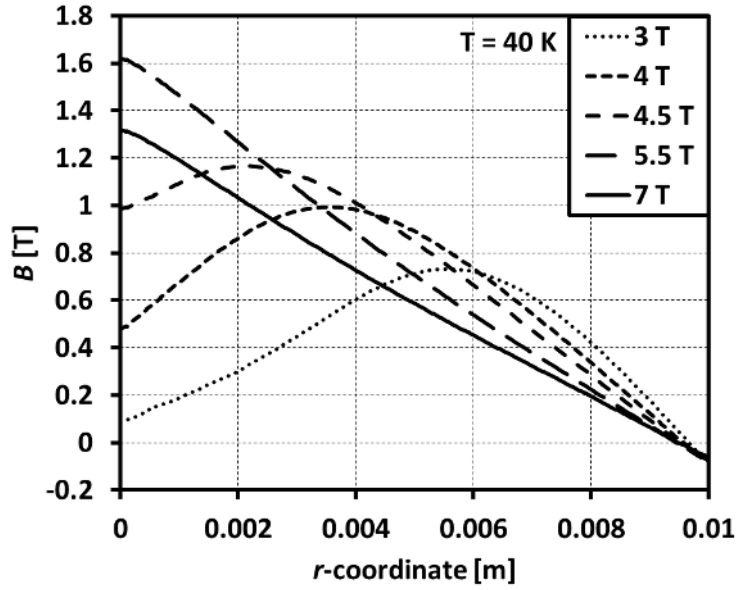
50 kA/cm<sup>2</sup> and  $B_{t,max} = 2$  T at 77 K, as well as such jumps (“giant flux leaps”) in the measured trapped field with only a small increase in the applied field [7,24,25].

It is also important to note that the maximum trapped field  $B_t = 3.4$  T for  $B_{app} = 6.25$  T for the high  $J_c$  sample is larger than the permissible value based on the simplistic CSM prediction, which suggests the field trapped at the centre is  $\leq \frac{1}{2}B_{app}$  for ZFC in the case of an infinitely long slab. Applying the Biot-Savart law to such a geometry, and assuming the CSM, would suggest that  $B_{app}$  should be 4 times the trapped field at the surface for full magnetization of the superconductor. For this particular sample geometry, where the ratio of thickness/diameter is  $\frac{1}{2}$ , an applied field of 3.276 times the surface trapped field would be required to fully magnetize the sample. This required applied field tends logarithmically to 2 times in the case of a thin sheet, where the central field can be assumed to be equal to the surface field. The same result is found for the ultra-high  $J_c$  sample, where  $B_t = 3.7$  T for  $B_{app} = 6.25$  T and  $B_t = 3.75$  T for  $B_{app} = 6.5$  T.

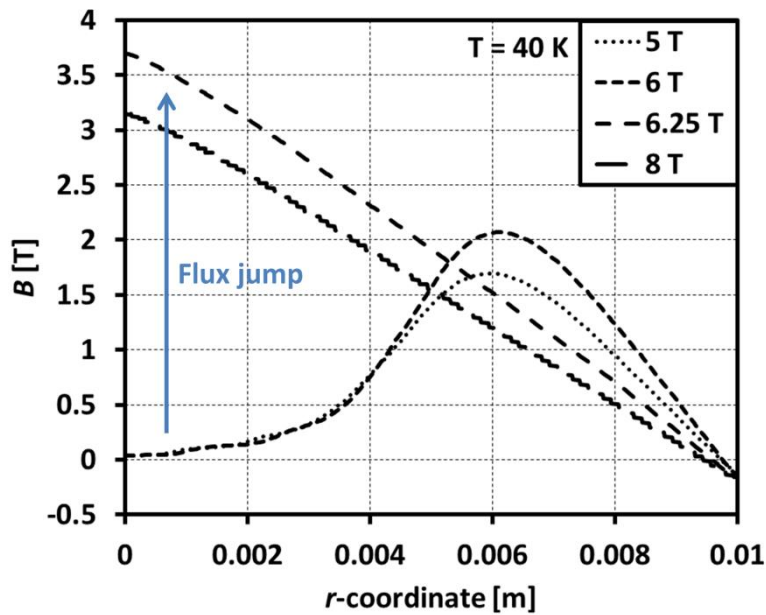
Furthermore, ordinarily for samples with increased  $J_c$ , the activation field (the applied pulsed field required to fully magnetise the sample [29]) also increases due to the stronger pinning forces that need to be overcome for the magnetic flux to fully penetrate the sample. In the case of the high and ultra-high  $J_c$  samples here, the flux jumps that occur act to reduce the activation field from its expected value, while allowing the sample to be fully magnetized with a high trapped field.

Fig. 5 shows the numerical simulation results for the trapped magnetic field profile across the top surface of the low  $J_c$  sample ( $z = 0.1$  mm) for increasing  $B_{app}$  between 3 T and 7 T for  $T_{op} = 40$  K. No flux jumps are observed, and the magnetic field penetration (and resultant trapped field) steadily increases with increasing  $B_{app}$ , until the sample is fully magnetized when  $B_{app} = 5.5$  T. Further increases in  $B_{app}$  above this value results in full magnetization, but a reduced maximum trapped field, consistent with previous experimental results observed by the authors [26,29,45], because of a larger temperature rise due to the higher applied field. Fig. 6 shows the same simulated trapped field profiles for the high  $J_c$  sample ( $z = 0.1$  mm) for increasing  $B_{app}$  between 3 T and 7 T for  $T_{op} = 40$  K. As shown in Fig. 4, the trapped field profile suddenly between  $B_{app} = 6$  T and 6.25 T, to a conical (fully magnetized) trapped field profile from a peak-valley shape (partially magnetized), again qualitatively consistent with the experimental results presented in [7,24,25]. One obvious difference between those experimental results and these simulated results is the height of the peak in the partially magnetized state, which can be explained by the different magnetizing fixture used: in [7,24,25], a split coil of smaller radius is used as the magnetizing fixture, for which the magnetizing mechanism is different in that, instead of flux penetrating from the periphery (or edge) of the bulk, the flux penetrates from the top/bottom surfaces [46,47].





**Figure 5.** Numerical simulation results for the trapped magnetic field profile across the top surface of the low  $J_c$  sample ( $z = 0.1$  mm) for increasing  $B_{app}$  between 3 T and 7 T for  $T_{op} = 40$  K. No flux jumps are observed.



**Figure 6.** Numerical simulation results for the trapped magnetic field profile across the top surface of the high  $J_c$  sample ( $z = 0.1$  mm) for increasing  $B_{app}$  between 5 T and 8 T for  $T_{op} = 40$  K. A large increase in the trapped field, due to flux jumps, is observed when increasing the applied field from 6 T to 6.25 T.

In order to study the magnetic flux dynamics in more detail, Fig. 7 shows the trapped field measured at three discrete locations above the top surface of the bulk (again at  $z = 0.1$  mm): centre, +4 mm, and +8 mm (2 mm from the edge of the 20 mm diameter sample). Figs. 7(a)-(c) show the change in time of the field calculated at each point as the pulse is applied, then removed, for the low  $J_c$  sample for  $B_{app} = 3, 4.5,$  and 5 T, respectively. Again, these results are consistent with CSM predictions and

the experimentally observed results in [7,24,25] for lower  $J_c$ , standard YBCO samples. The combination of a large applied field near the edge of the sample and the associated temperature rise due to the rapid movement of magnetic flux into the sample results in a localised, suppressed  $J_c$ , and the field at the +8 mm point from the centre almost follows the applied field for increasing  $B_{app}$  values. Figs. 7(d)-(f) shows similar plots for the high  $J_c$  sample, where flux jumps act to assist the PFM process, resulting in a sudden, large increase in the trapped field at the centre of the sample. When  $B_{app} = 5$  T, no flux jump is observed in the high  $J_c$  sample, and the magnetic flux dynamics are similar to those for the low  $J_c$  sample in Fig. 7(a). However, when  $B_{app} = 6$  T, as shown in Fig. 7(e), a flux jump is observed at +4 mm between  $t = 4.5$ -5 ms, but there is no change at the centre of the sample. Increasing the applied field a further 0.25 T results in a second flux jump between  $t = 11.5$ -12 ms, as shown in Fig. 7(f). Consequently, a large and sudden increase in magnetic field is seen at the centre, resulting in full magnetization of the sample.

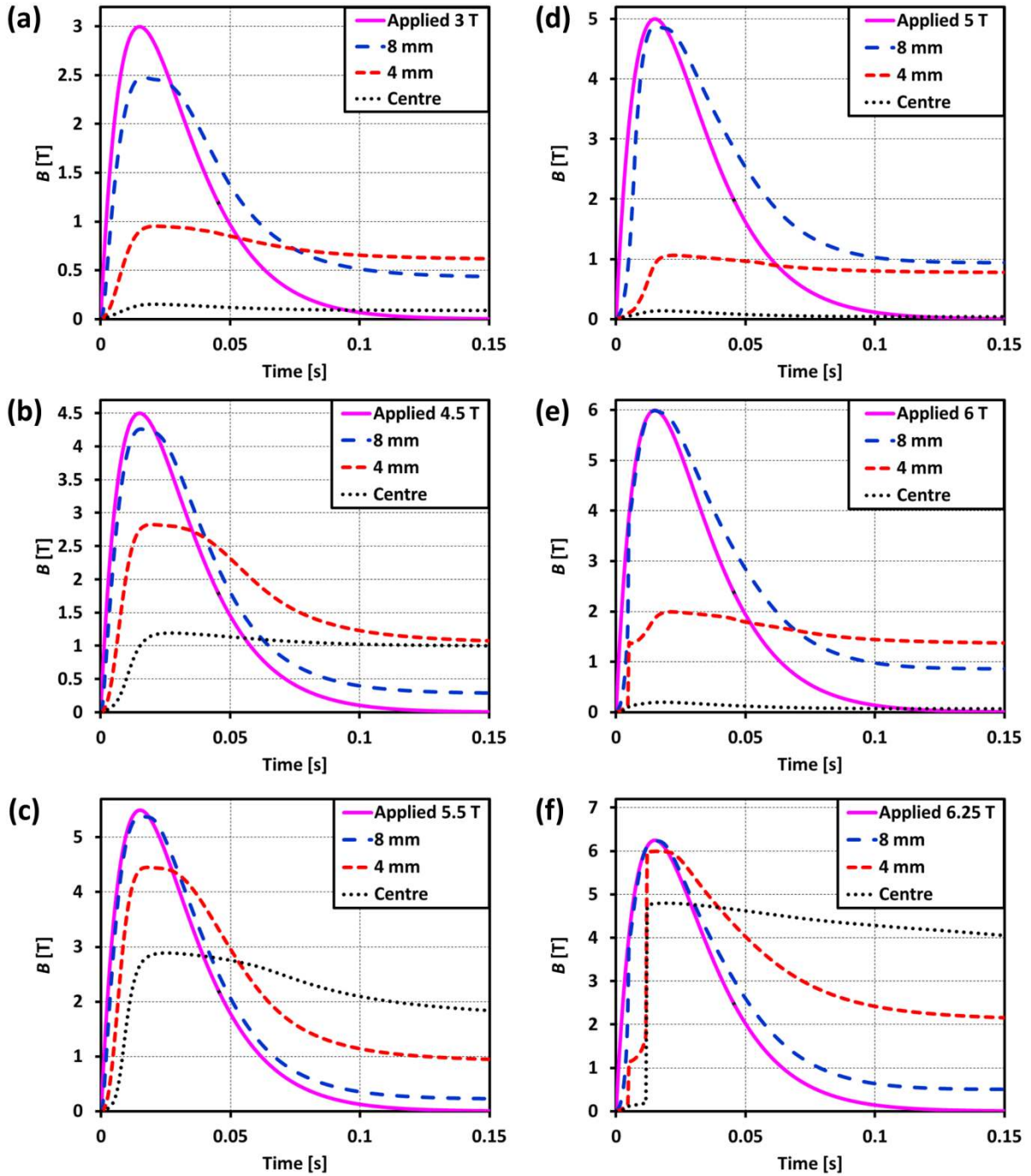


**Figure 7.** Trapped field measured at three discrete locations above the top surface of the bulk ( $z = 0.1$  mm): centre, +4 mm, and +8 mm (2 mm from the edge of the 20 mm diameter sample). Panels (a)-(c) show the change in time of the field calculated at each point for the low  $J_c$  sample for  $B_{app} = 3$ , 4.5, and 5 T, respectively. (d)-(f) show the change in time of the field calculated at each point for the high  $J_c$  sample for  $B_{app} = 5$ , 6, and 6.25 T, respectively.

Fig. 8(a) shows the average temperature,  $T_{ave}$ , of the low  $J_c$  sample during the pulse until the applied field reaches its peak value and Fig. 8(b) shows the sample's average critical current density,  $J_{c,ave}$ . Both  $T_{ave}$  and  $J_{c,ave}$  are calculated by integrating  $T$  and  $J_c$ , respectively, over the cross-sectional area of the bulk, and the result is divided by this area. There is a smooth increase in temperature and decrease in  $J_c$  due to the magnetic flux penetration during the rising pulse. Since the time constant,  $\tau$ , of each pulse is the same, a higher  $B_{app}$  value results in higher  $dB/dt$  and larger field penetration, resulting in a larger temperature rise and further suppression of  $J_c$ . Figs. 9(a) and (b) show the same plots for the high  $J_c$  sample. For  $B_{app} = 5$  T for the high  $J_c$  sample, where no flux jump occurs, there is a similar smooth increase in  $T_{ave}$  and reduction in  $J_{c,ave}$ . The flux jumps that occur for higher applied fields,  $B_{app} = 6, 6.25$  T, are accompanied by a large and sudden temperature rise and a simultaneous, mirrored reduction in  $J_{c,ave}$ . The temperature rise during PFM takes place adiabatically [3], because a large proportion of the heat generation takes place instantaneously and the cooling power is finitely limited. The low thermal conductivity of the bulk also seriously affects the thermal and electromagnetic responses, for which the thermal diffusion is much slower than the magnetic diffusion. When modelling typical experimental conditions, and for a typical rise time of  $\tau \approx 10$  ms of the applied pulse, the magnetic flux propagation can be an order of magnitude or higher faster than the heat propagation [48]. Another example of such behaviour can be observed in Fig. 21 in [26].

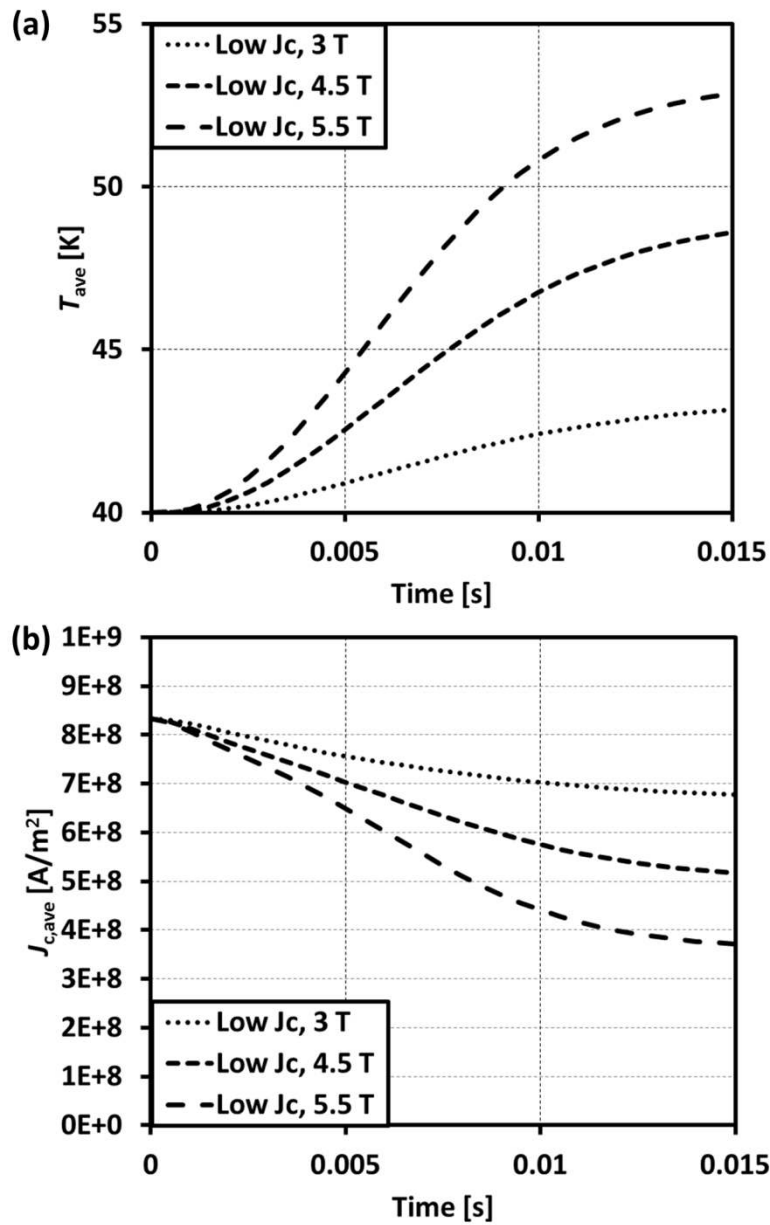


**Figure 8.** (a) Average temperature,  $T_{ave}$ , of the low  $J_c$  sample during the pulse, until the applied field reaches its peak value, for  $B_{app} = 3, 4.5$  and  $5.5$  T. (b) The sample's average critical current density,  $J_{c,ave}$ , over the same period of time for the same applied fields.

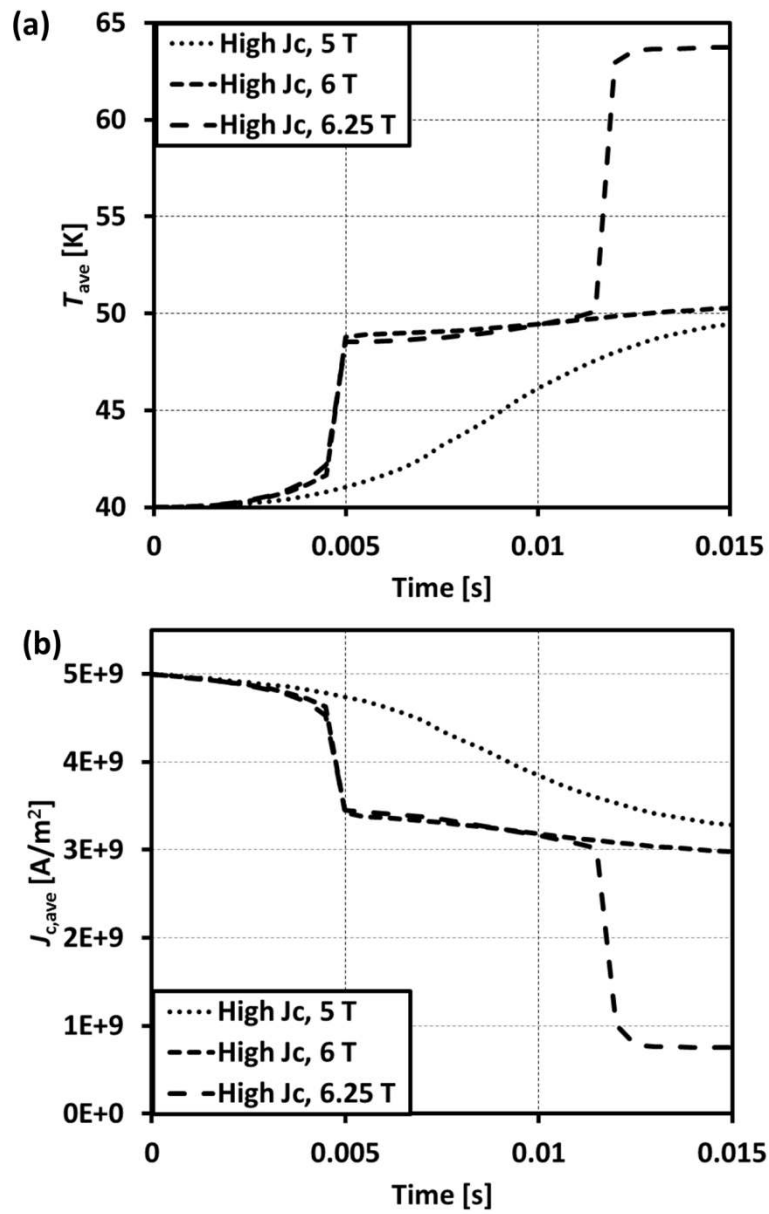


**Figure 9.** (a) Average temperature,  $T_{ave}$ , of the high  $J_c$  sample during the pulse, until the applied field reaches its peak value, for  $B_{app} = 5, 6$  and  $6.25$  T. (b) The sample's average critical current density,  $J_{c,ave}$ , over the same period of time for the same applied fields.

In [24,25], it was speculated that a large Lorentz force, given by  $F_L = \mathbf{J} \times \mathbf{B}$ , acting on the magnetic flux penetrating the sample during the PFM process is a cause of the flux jumps into the sample. In order to clarify this hypothesis, Fig. 10 shows the calculated maximum Lorentz force density in each of the bulk samples, until the pulse reaches its peak value, for (a)  $B_{app} = 5$  T, (b)  $B_{app} = 6$  T, and (c)  $B_{app} = 7$  T. Here, the Lorentz force density in the  $-r$  direction is calculated, which drives the magnetic flux towards the centre of the sample, and is given by  $-J\mu_0 H_z$ . For  $B_{app} = 5$  T, no flux jumps occur for the low, normal and high  $J_c$  samples, but there is a flux jump between  $t = 6.5$ -7 ms for the ultra-high  $J_c$  sample. As shown in Fig. 10(a), the maximum Lorentz force density in the sample increases with  $J_c$ , and the flux jump in the ultra-high  $J_c$  sample is preceded firstly by a large  $F_L$ , followed by a slight reduction in  $F_L$ , which rapidly reduces when the flux jump occurs. When  $B_{app}$  is increased to 6 T, as shown in Fig. 10(b), this behaviour becomes more pronounced. Finally, when  $B_{app}$  is increased to 7 T, as shown in Fig. 10(c), two flux jumps are observed for the high and ultra-high  $J_c$  samples, with the latter one causing flux to jump all the way into the centre of the sample. This secondary flux jump is preceded by the attainment of a large  $F_L$  value, comparable to the  $F_L$  value at which the first flux jump occurred. These results provide good evidence that the flux leap in high- $J_c$  bulk superconductors is due to the large Lorentz force acting on the magnetic flux penetrating the sample, which causes flux to jump further into the sample, resulting in a sudden and large increase in temperature and reduction in  $J_c$  (as shown in Fig. 9). The maximum value of  $J/J_c$  during the pulse rise time was also examined to discern whether this is a cause of the flux jumps, and no correlation between  $J/J_c$  and the flux jumps was observed. In fact, in the case of the normal  $J_c$  bulk,  $J/J_c$  exceeded 2 during the pulse rise time for  $B_{app} = 6, 7$  T, for example, with no flux jumps observed.

Hence, if the  $F_L$  value is large enough, a flux jump to the centre of the sample can be induced that can fully magnetize a sample, with a reduction in the required activation field, which is significant for practical applications as such flux jumps could be exploited to provide higher trapped fields, whilst reducing the cost and size of the magnetizing fixture. This numerical simulation framework provides a flexible and cost-effective method for analysing and optimising different magnetizing fixtures, as well as examining the effect of different  $J_c$  and pinning characteristics of other families of superconducting materials and/or materials made from different processing techniques.

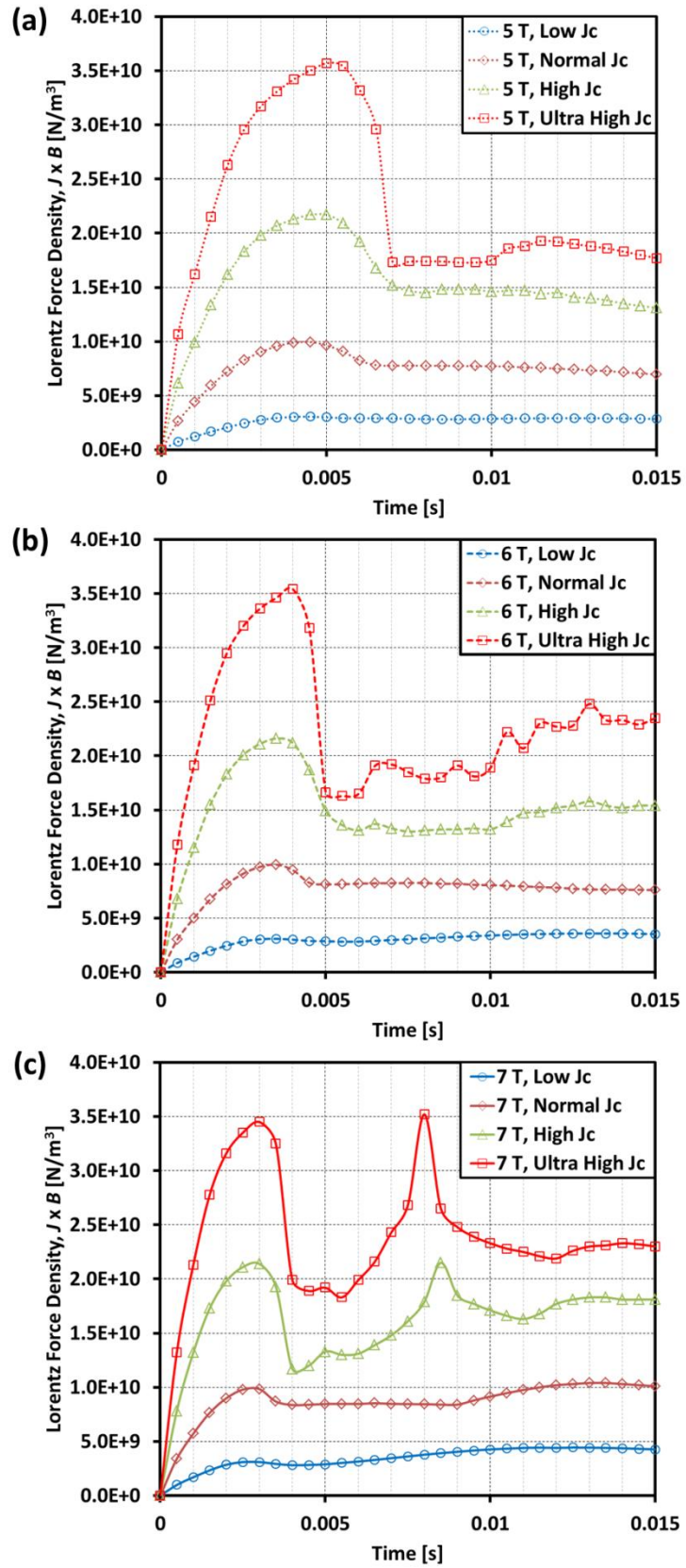


**Figure 10.** Calculated maximum Lorentz force density,  $J \times B$ , in the bulk samples, until the pulse reaches its peak value, for (a)  $B_{app} = 5$  T, (b)  $B_{app} = 6$  T, and (c)  $B_{app} = 7$  T.



### 3. Conclusion

So-called “giant flux leaps” have been observed by a number of research groups investigating PFM of bulk high-temperature superconductor, where flux jumps occur in the superconductor, and magnetic flux suddenly intrudes into the centre of the sample. This phenomenon is assistive to the PFM process and results in a large increase in the measured trapped field at the centre of the top surface and full magnetization of the sample. In this paper, a 2D axisymmetric finite-element model implementing the  $\mathbf{H}$ -formulation, with a modified  $E$ - $J$  power law characteristic representing the normal state resistivity of the superconductor when  $J > J_c$ , is used to qualitatively reproduce this phenomenon to good effect. By simply inserting a bulk sample of high  $J_c$ , as found in high quality standard samples and neutron-irradiated ones, such “giant flux leaps” or flux jumps are observed in the model, due to the large Lorentz force,  $F_L$ , generated during the PFM process that drives the magnetic flux into the sample. The flux jumps are accompanied by a large and sudden temperature rise, and a simultaneous, mirrored reduction in  $J_{c,ave}$ . The maximum value of  $J/J_c$  during the pulse rise time was also examined to discern whether this is a cause of the flux jumps, and no correlation between  $J/J_c$  and the flux jumps was observed. The numerical simulation framework is extremely flexible and provides a cost-effective method for analysing and optimising different magnetizing fixtures, as well as examining the effect on samples of different  $J_c$  and pinning characteristics, to exploit such flux jumps to enhance the trapped field in practical, bulk superconductor applications.

### Acknowledgments

Dr Mark Ainslie would like to acknowledge the support of a Royal Academy of Engineering Research Fellowship. The authors would like to thank Archie Campbell, University of Cambridge, for his useful discussions.

### References

- [1] Tomita M and Murakami M 2003 Nature 421 517-20
- [2] Durrell J H et al 2014 Supercond. Sci. Technol. 27 082001
- [3] Ainslie M D and Fujishiro H 2015 Supercond. Sci. Technol. 28 053002
- [4] Nariki S, Sakai N and Murakami M 2005 Supercond. Sci. Technol. 18 S126-30
- [5] Weinstein R, Sawh R-P, Parks D and Mayes B 2012 Nucl. Instrum. Meth. B 272 284-290
- [6] Weinstein R et al 2000 Physica C 341-48 1415-18
- [7] Weinstein R et al 2015 IEEE Trans. Appl. Supercond. 25-3 6601106
- [8] Hull J and Murakami M 2004 Proc. IEEE 92 1705-18
- [9] Murakami M 2007 Int. J. Appl. Ceram. Technol. 4 225–41
- [10] Zhou D et al 2012 Supercond. Sci. Technol. 25 103001
- [11] Zhang Y et al 2016 Supercond. Sci. Technol. 29 044005
- [12] Yokoyama K et al 2003 IEEE Trans. Appl. Supercond. 13-2 1592-95
- [13] Nakamura T et al 2007 Concepts Magn. Reson. B 31B 65
- [14] Nakamura T et al 2015 J. Magn. Reson. 259 68-75
- [15] Fujishiro H, Itoh Y, Yanagi Y and Nakamura T 2015 Supercond. Sci. Technol. 28 095018

- [16] Saho N et al 2009 Physica C 469 1286-9
- [17] Nishijima S et al 2009 IEEE Trans. Appl. Supercond. 19-3 2257-60
- [18] Fujishiro H et al 2005 Physica C 445-8 334-8
- [19] Itoh Y and Mizutani U 1997 Japan J. Appl. Phys. 35 2114-25
- [20] Itoh Y, Yanagi Y and Mizutani U 1997 J. Appl. Phys. 82 5600-11
- [21] Ikuta H et al 2002 Supercond. Sci. Technol. 15 606-12
- [22] Mizutani U et al 1998 Appl. Supercond. 6 235-46
- [23] Yanagi Y et al 2005 Supercond. Sci. Technol. 18 839-49
- [24] Weinstein R et al 2015 Appl. Phys. Lett. 107 152601
- [25] Weinstein R et al 2016 J. Appl. Phys. 119 133906
- [26] Ainslie M D et al 2016 Supercond. Sci. Technol. 29 074003
- [27] Cha Y S 2005 Chin. J. Phy. 43 681-92
- [28] COMSOL, Inc. ([www.comsol.com](http://www.comsol.com))
- [29] Ainslie M D et al 2014 Supercond. Sci. Technol. 27 065008
- [30] Plummer C J G and Evetts J E 1987 IEEE Trans. Magn. 23 1179-82
- [31] Rhyner J 1993 Physica C 212 292-300
- [32] Duron J et al 2004 Physica C 401 231-5
- [33] Duron J et al 2007 Supercond. Sci. Technol. 20 338-44
- [34] Xia J and Zhou Y 2015 Cryogenics 69 1-9
- [35] Zou J et al 2015 Supercond. Sci. Technol. 28 075009
- [36] Zou S, Zermeno V M R and Grilli F 2016 IEEE Trans. Appl. Supercond. 26 4702405
- [37] Brandt E H 1995 Rep. Prog. Phys. 58 1465-1594
- [38] Hu D et al 2015 Supercond. Sci. Technol. 28 065011
- [39] Hu D et al 2016 IEEE Trans. Appl. Supercond. 26 6600906
- [40] Jirsa M, Púst L, Dlouhý D and Koblishka M R 1997 Phys. Rev. B 55 3276-84
- [41] Fujiyama K, Shiraishi R and Ohsaki H 2005 Physica C 426-31 681-7
- [42] Shiraishi R and Ohsaki H 2006 IEEE Trans. Appl. Supercond. 16 1794-7
- [43] Zhang M and Coombs T A 2012 Supercond. Sci. Technol. 25 015009
- [44] Fujishiro H et al 2011 Supercond. Sci. Technol. 24 105003
- [45] Ainslie M D et al 2015 Supercond. Sci. Technol. 28 125002
- [46] Xu Z et al 2012 Supercond. Sci. Technol. 25 025016
- [47] Fujishiro H, Naito T and Oyama M 2011 Supercond. Sci. Technol. 24 075015
- [48] Fujishiro H and Naito T 2010 Supercond. Sci. Technol. 23 105021